Inorganic Chemistry

Article

pubs.acs.org/IC

Donor Properties of a New Class of Guanidinate Ligands Possessing Ketimine Backbones: A Comparative Study Using Iron

Arnab K. Maity, Alejandro J. Metta-Magaña, and Skye Fortier*

Department of Chemistry, University of Texas at El Paso, El Paso, Texas 79968, United States

Supporting Information

ABSTRACT: Addition of 1 equiv of LiN=C^{t}Bu$_2$ or LiN=Ad (Ad = 2-adamantyl) to the aryl carbodiimide *C*(NDipp)$_2$ (Dipp = 2,6-diisopropylphenyl) readily generates the lithium ketimine-guanidinates Li(THF)$_2$[(X)C(NDipp)$_2$] (X = N=C^{t}Bu$_2$ (**1-^{t}Bu**), N=Ad (**1-Ad**)) in excellent yields. These new ligands can be readily metalated with iron to give the *N*,*N*′-bidentate chelates [{(X)*C*(NDipp)$_2$}-FeBr]$_2$ (X = N=C^{t}Bu$_2$ (**5-^{t}Bu**), N=Ad (**5-Ad**)), in which the ketimines behave as noncoordinating backbone substituents. In an effort to understand the potential electronic contributions of the ketimine group to the ligand architecture, a thorough structural and electronic study was conducted comparing the features and properties of **5-^{t}Bu** and **5-Ad** to their guanidinate and amidinate analogues [{(X)*C*(NDipp)$_2$}FeBr]$_2$ (X = ^{i}Pr$_2$N (**6**), ^{t}Bu (**7**)). Solid-state structural analyses indicate little electronic contribution from the *N*-ketimine nitrogen atom, while solution-phase electronic absorption spectra of **5-^{t}Bu** and **5-Ad** are qualitatively similar to the amidinate complex **7**. Yet, electrochemical measurements do show the donor properties of the ketimine-guanidinate in **5-^{t}Bu** to be intermediate between its guanidinate and amidinate counterparts in **6** and **7**. Preliminary reactivity studies also show that the reduction chemistry of **5-^{t}Bu** diverges significantly from that of **6** and **7**. Treatment of **5-^{t}Bu** with excess magnesium or 1 equiv of KC$_8$ leads to the formation of the Fe(I)−Fe(I) complex [{μ-(^{t}Bu$_2$C=N)*C*(NDipp)$_2$}$_2$Fe$_2$] (**11**), which possesses an exceedingly short Fe=Fe bond (2.1516(5) Å), while neither **6** nor **7** forms dinuclear complexes upon reduction. This result demonstrates that ketimine-guanidinates do not simply behave as amidinate variants but can contribute to distinctive metal chemistry of their own.

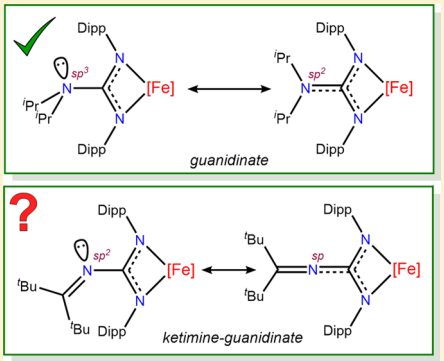

INTRODUCTION

Numerous review articles have been written in recent years regarding the features and coordination chemistry of formamidinate, amidinate, and guanidinate ligands (in both their neutral and anionic forms), documenting a surge in their popularity that has occurred over the past decade.[1−4] These amidoimines have become attractive ligand platforms owing, in part, to the ease in which they can be accessed, most commonly through an array of synthetic routes that utilize generally straightforward procedures with simple starting materials, which allows for ready customization and high modularity.[2] Additionally, amidoimine ligands are highly compatible with a wide range of elements, a characteristic that has given rise to a multitude of s-, p-, d-, and f-block complexes.[1−16] Described in some cases as "steric cyclopentadienyl equivalents",[2] these ligands can kinetically stabilize metals in very low oxidation states by blocking disproportionation pathways.[1] Conversely, amidoimines are sufficiently electron donating as to support metals in high oxidation states or unusually low coordination geometries.[2,5,15]

While formamidinates, amidinates, and guanidinates all share the basic Y-shaped form [XC(NR)$_2$]$^-$ (X = H, alkyl, NR$_2$, respectively), notable differences between these ligand subclasses do exist. When the ligand has an alkyl group or hydrogen in the backbone "X" position, a 1,3-diazaallyl form dominates, which largely limits π-conjugation to the two nitrogen atoms of the XCN$_2$ core (Scheme 1, **A** and **B**). On the other hand, when "X" is an amine, the π-conjugation can be extended to the nitrogen atom of the backbone amino group, permitting a third, iminium-diamido resonance form (Scheme 1, **C**).[1,5,17] Contributions from resonance structure **C**, i.e., the degree of delocalization within the CN$_3$ core, can be readily seen by X-ray crystallography. In the solid state, guanidinates are often found to exhibit nearly equivalent C−N distances within the CN$_3$ moiety and bond sum angles about the backbone amino nitrogen that approach 360°.[3,14] This ligand

Scheme 1. 1,3-Diazaallyl Resonance Forms A and B of the Amidoimines; C Represents the Canonical Iminium-Diamido Form Only Accessible to Guanidinates

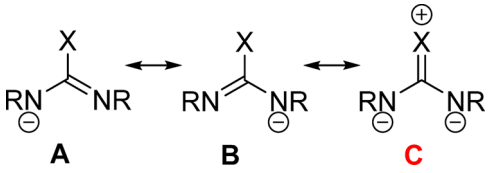

Received: August 8, 2015
Published: September 30, 2015

DOI: 10.1021/acs.inorgchem.5b01815
Inorg. Chem. 2015, 54, 10030−10041

electronic structure augments the electron-donating properties of guanidinates, making them better donors than their amidinate and formamidinate counterparts.[1,5] Consequently, guanidinates are generally regarded as competent electron donors, a concept reinforced by the discovery that guanidinates also exhibit superior donating abilities over their β-diketiminate cousins.[14]

In our group, we have been exploring guanidinate ligand design with the purpose of engineering guanidinate ligands that are both encumbering and highly electron-rich.[16] We reasoned that the donating abilities of guanidinates could be further enhanced by replacing the $-NR_2$ amine backbone for an $-N{=}CR_2$ ketimine functionality. It has been demonstrated that, as monoanionic ligands, ketimides are strong σ- and π-donors capable of supporting metals in unusually high oxidation states (e.g., $M^{IV}(N{=}C^tBu_2)_4$, M = Fe, Co).[18,19] As a backbone substituent, these electronic characteristics well-situate the *N*-ketimine lone pair for π-conjugation into the guanidinate CN_3 core, favoring an iminium-diamido resonance form (Scheme 2, **F**). In principle, for a "ketimine-guanidinate", a fourth, carbonium-diamido resonance (Scheme 2, **G**) would also be accessible, adding further diamido character to the overall ligand electronic structure. However, preliminary empirical evidence seems to contradict this supposition. To the best of our knowledge, only two ketimine-guanidinate ligands have been reported, namely, $[(^tBu_2C{=}N)C(NAr^*)_2]^-$ (Ar* = 2,6-bis(diphenylmethyl)-4-*tert*-butylphenyl) and $[(Me_2C{=}N)C(N^iPr_2)_2]^-$, wherein neither shows any significant structural evidence of *N*-ketimine π-conjugation.[16,20] In the former, the lack of an observable *N*-ketimine π-contribution may simply be a consequence of steric crowding within the encumbered guanidinate framework. Alternatively, in either example, crystal packing forces may also play a role.

Scheme 2. Possible Resonance Structures of Ketimine-Functionalized Guanidinates

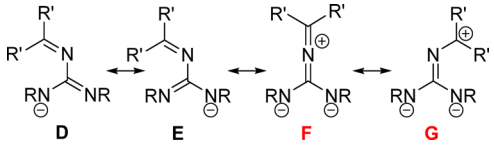

It must be kept in mind that structural analyses, while important, are but one metric for assessing the delocalization phenomenon, and effects from the participation of the *N*-ketimine lone pair in the guanidinate π-system can manifest themselves in other detectable ways. Therefore, in an effort to evaluate the effect of replacing the amine backbone of a guanidinate for a ketimine group, we have performed a comprehensive study comparing the structural and electronic properties of metalated ketimine-guanidinates to their well-defined amidinate and guanidinate analogues. Specifically, we have chosen to compare the iron series $[\{(X)C(NDipp)_2\}FeBr]_2$ (X = N=C^{t}Bu$_2$ (**5-^{t}Bu**), N=Ad (**5-Ad**), N^{i}Pr$_2$ (**6**), ^{t}Bu (**7**); Dipp = 2,6-diisopropylphenyl) wherein the complexes are differentiated only by their backbone group. For a basis of comparison, all compounds have been fully characterized by X-ray crystallography; cyclic voltammetry; and ^{1}H NMR, IR, and UV−vis spectroscopies. Finally, a comparison of the reduction chemistry of **5-^{t}Bu** to **6** and **7** is also presented, revealing distinct structure−reactivity relationships.

RESULTS AND DISCUSSION

Ligand Synthesis and Characterization. For this study, the ketimine substituent $-N{=}C^tBu_2$ was chosen because of its demonstrated abilities as a good electron donor;[18,19] although, as it is bulky and can introduce secondary steric effects, an additional related, but sterically nonobtrusive, ketimine was desired. Thus, we selected −N=Ad (Ad = 2-adamantyl), which can be considered a "clipped" or "pinned back" counterpart to $-N{=}C^tBu_2$. Addition of 1 equiv of LiN=C^{t}Bu$_2$ or LiN=Ad to $(DippN)_2C$ in THF with heating at 65 °C for 1 day smoothly generates the lithium ketimine-guanidinates $Li(THF)_2[(X)C(NDipp)_2]$ (X = N=C^{t}Bu$_2$ (**1-^{t}Bu**), N=Ad (**1-Ad**)) (Scheme 3). These reactions can be readily performed on multigram scales, affording the products cleanly in 92% and 76% yields, respectively. Both **1-^{t}Bu** and **1-Ad** are white solids that are partially soluble in aliphatic solvents, such as hexanes, but soluble in aromatic and ethereal solvents.

The room-temperature ^{1}H NMR spectrum of **1-^{t}Bu** in C_6D_6 is well-resolved and exhibits a sharp singlet at 1.03 ppm that corresponds to the *tert*-butyl protons of its ketimine fragment. The methine and diastereotopic methyl protons of the peripheral isopropyl groups are readily identified by a septet

Scheme 3. Synthesis of Ketimine-Guanidinate Ligands 4-^{t}Bu and 4-Ad

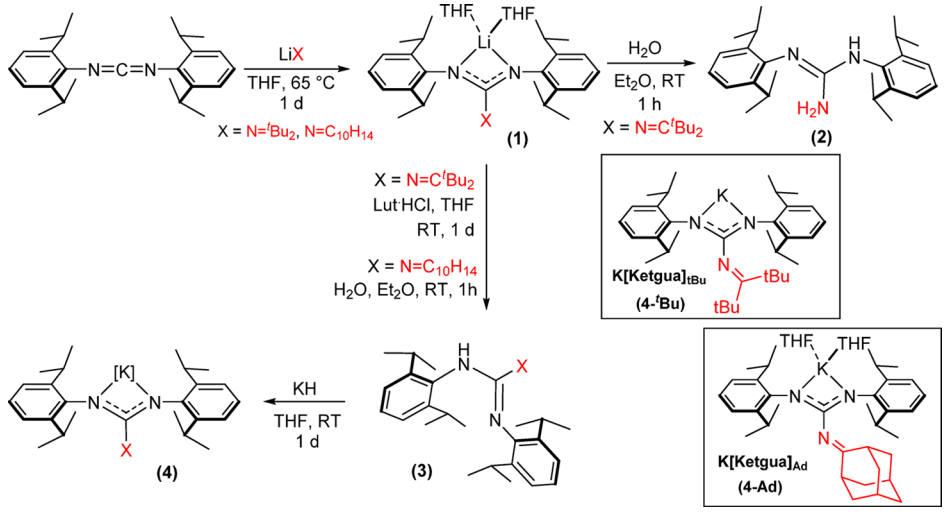

DOI: 10.1021/acs.inorgchem.5b01815
Inorg. Chem. 2015, 54, 10030−10041

at 4.07 ppm accompanied by two doublets at 1.28 and 1.52 ppm in a 4:12:12 ratio, respectively. Additionally two peaks at 1.37 and 3.55 ppm, integrating to eight protons each, indicate the presence of two lithium-coordinated molecules of THF. Furthermore, the $^{7}Li\{^{1}H\}$ NMR spectrum displays one single resonance at 1.61 ppm. These assignments were further confirmed by preliminary X-ray data that allowed for atom connectivity determination (Figure S5 in the Supporting Information (SI)).

On the other hand, the room-temperature ^{1}H NMR spectrum of **1-Ad** exhibits a set of broad peaks suggestive of fluxional solution-phase behavior, a phenomenon that is not uncommon to guanidinates.[3,4] Consistent with this, the room-temperature $^{7}Li\{^{1}H\}$ NMR spectrum shows two peaks at −0.9 and 2.7 ppm. Cooling a toluene-d_8 solution of **1-Ad** to −50 °C resolves the ^{1}H NMR spectra into a complicated series of resonances, indicative of the presence of multiple isomeric forms at low temperature, while heating a toluene-d_8 solution of **1-Ad** to 50 °C results in coalescence to one peak set (Figures S7 and S8 in the SI).

For the purposes of our studies, it was important to synthesize the potassium derivatives of **1** (vide infra). A lithium for potassium swap in guanidinates is commonly accomplished by hydrolysis of the lithium salt followed by deprotonation of the resulting *H*guanidine by a potassium base such as KH or $KN(SiMe_3)_2$.[4] Accordingly, addition of water to an ethereal solution of **1-Ad** readily gives (Ad═N)*C*(NDipp)(NHDipp) (**3-Ad**) (Scheme 3), as confirmed by NMR spectroscopy and mass spectrometry. Treatment of **1-^{t}Bu** with water produced a white solid upon workup that was found to be sparingly soluble in aromatic solvents. Surprisingly, clearly absent from the ^{1}H NMR spectrum were any resonances corresponding to the protons of a *tert*-butyl group, thus suggesting full loss of the ketimine functionality. Instead, in its place, a new signal is observed at 3.01 ppm, integrating to two protons, corresponding to a newly formed $-NH_2$ backbone to give the guanidine $(NH_2)C$(NDipp)(NHDipp) (**2**) (Scheme 3 and Figure S12 in the SI). The ^{1}H NMR spectrum of this material in toluene-d_8 at −40 °C gives a set of sharp peaks fully consistent with the proposed formulation for **2** (Figure S13 in the SI). Altogether, these data suggest that the ketimine group of **1-^{t}Bu** upon exposure to water is hydrolyzed. In line with this, the exposure of a C_6D_6 solution of **1-^{t}Bu** to moist air confirms the formation of hexamethylacetone as the sole ketimine hydrolysis product in the conversion of **1-^{t}Bu** to **2** (Figures S17 and S18 in the SI). Finally, the structural composition of **2** was unambiguously confirmed via X-ray crystallographic analysis of a single crystal grown from a concentrated benzene solution (Figure S16 in the SI).

Successful protonation of **1-^{t}Bu** was accomplished by treating it with an anhydrous proton source, specifically lutidinium hydrochloride, in THF to give the desired product ($^{t}Bu_2C$═N)*C*(NDipp)(NHDipp) (**3-^{t}Bu**) (Scheme 3) cleanly and in good yield. The room-temperature ^{1}H NMR spectrum of **3-^{t}Bu** features many broad resonances, while that of **3-Ad** displays an assortment of broad and sharp peaks. In either case, as with **1-Ad**, this can be attributed to dynamic conformational and tautomeric interconversion in solution that is frequently encountered with guanidines and related systems.[3,21] Accordingly, cooling a toluene-d_8 solution of **3-^{t}Bu** to −60 °C or **3-Ad** to −50 °C simplifies their ^{1}H NMR spectra (Figures S20 and S25 in the SI, respectively). At these temperatures, both **3-^{t}Bu** and **3-Ad** each coincidentally adopt two predominant isomeric forms, in respective 70:30 and 60:40 ratios, as revealed by the presence of two characteristic N*H* resonances in each of their respective ^{1}H NMR spectra.

The IR spectra (KBr pellet) of **3-^{t}Bu** and **3-Ad** display telltale N−H stretches[3] at 3423 and 3443 cm^{-1}, respectively. Interestingly, these values, especially that of **3-^{t}Bu**, are very close to that of the related amidine (^{t}Bu)*C*(NDipp)(NHDipp) (3416 cm^{-1})[22] but are set apart from the guanidine ($^{i}Pr_2N$)*C*(NDipp)(NHDipp) (3364 cm^{-1})[23] by ca. 60−80 wavenumbers. Broadly, this appears to suggest a greater structural relation between the ketimine-guanidines **3-^{t}Bu** and **3-Ad** to amidines than to guanidines; however, as the N−H stretching frequency of amidines widely ranges, this correlation alone is not conclusive.[3]

Compounds **3-^{t}Bu** and **3-Ad** are readily deprotonated by addition of a slight excess of KH in THF at room temperature to give $[K(THF)_n][(X)C(NDipp)_2]$ (X = N═C$^{t}Bu_2$, n = 0 (**4-^{t}Bu**); N═Ad, n = 2 (**4-Ad**)) in nearly quantitative yields (Scheme 3). Both compounds are sparingly soluble in aliphatics, partially soluble in aromatic solvents, but highly soluble in THF. The ^{1}H NMR spectrum of **4-^{t}Bu** is unremarkable and qualitatively similar to **1-^{t}Bu**. Akin to its lithium analogue **1-Ad**, the room-temperature ^{1}H NMR spectrum of **4-Ad** in a C_6D_6/pyridine-d_5 (10:1) mixture also displays broad peaks; however, the observed signals correspond to only one isomeric form.

Synthesis and Characterization of Iron Ketimine-Guanidinates. For the purpose of this comparative study, the Fe(II) platform $[\{(X)C(NDipp)_2\}FeBr]_2$ was chosen as both the amidinate **7** and the closely related guanidinate iron chloride analogue $[\{(^{i}Pr_2N)C(NDipp)_2\}FeCl]_2$ (**6-Cl**) are well-known, are well-behaved, and have been thoroughly characterized by spectroscopic and structural methods.[24] In order to minimize intervening factors, such as those potentially introduced by differing halide groups, the guanidinate bromide derivative **6** was desired. Compound **6** was readily synthesized (eq 1) using procedures adapted from the reported synthesis of **6-Cl**, and its solid-state structure is shown in Figure 1.[24]

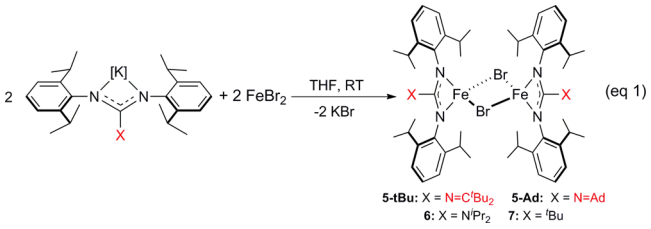

Attempts to synthesize the related Fe(II) ketimine-guanidinates **5-^{t}Bu** and **5-Ad** from the metathesis reaction of $FeBr_2$ with **1-^{t}Bu** or **1-Ad** were complicated by the difficult elimination of LiBr from the product mixtures. Instead, treating a THF solution of $FeBr_2$ with 1 equiv of **4-^{t}Bu** or **4-Ad** at room temperature smoothly generates **5-^{t}Bu** and **5-Ad** as mustard yellow solids in 81% and 72% yields, respectively (eq 1). Each complex exhibits moderate solubility in aliphatics, aromatic solvents, and diethyl ether but are fully soluble in THF. The ^{1}H NMR spectrum of **5-^{t}Bu** in C_6D_6 exhibits six paramagnetically shifted resonances at 21.8, 15.8, 9.5, 1.4, −10.7, and −11.1 ppm in a 4:4:18:12:2:12 ratio, respectively, consistent with a C_2 symmetric molecule in solution. Similarly, the ^{1}H NMR spectrum of **5-Ad** in C_6D_6 shows a series of 10 peaks at 21.10, 8.58, 7.19, 6.07, 4.86, 4.04, 3.30, 0.31, −5.51, and −9.98

DOI: 10.1021/acs.inorgchem.5b01815
Inorg. Chem. 2015, 54, 10030−10041

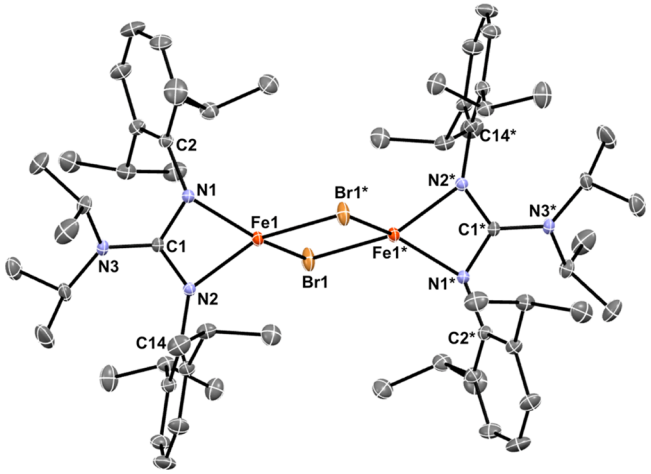

Figure 1. ORTEP diagram of **6** with 35% probability thermal ellipsoids. Hydrogen atoms are omitted for clarity. Asterisks denote symmetry-generated atoms.

ppm in a 4:2:2:4:4:12:4:2:12:2 ratio, respectively, also indicative of an adamantyl-inclusive C_2 symmetric molecule.

Single crystals of **5-^{t}Bu** were grown from a concentrated toluene solution stored at −25 °C for 2 days, while **5-Ad** was crystallized as the toluene solvate **5-Ad**·C_7H_8 from a concentrated toluene solution kept at −25 °C for several days. Complex **5-^{t}Bu** crystallizes in the orthorhombic space group *Pbca* and **5-Ad** in the monoclinic space group $P2_1/c$ with both solid-state molecular structures shown in Figure 2. The asymmetric units of **5-^{t}Bu** and **5-Ad** each contain one full [(X)C(NDipp)$_2$]FeBr monomeric unit that resides on an inversion center. Upon symmetry generation, a dimer is revealed possessing a bridging [Fe_2Br_2] diamond core, identical to that found for both **6** (Figure 1) and **7**.[24] As predicted by the ^{1}H NMR spectra, the [(X)C(NDipp)$_2$]$^-$ ligands exhibit a κ^2-coordination mode with each iron center bound between the two N_{Dipp} nitrogens.

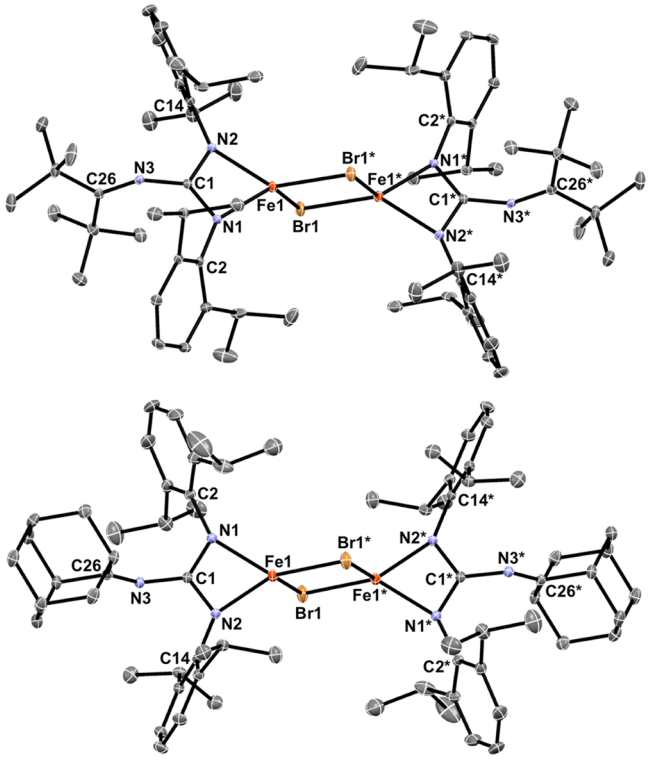

Figure 2. ORTEP diagram of **5-^{t}Bu** (top) and **5-Ad**·C_7H_8 (bottom) with 35% probability thermal ellipsoids. Hydrogen atoms and a cocrystallized molecule of toluene are omitted for clarity. Asterisks denote symmetry-generated atoms.

Notably, though, in the solid state, the ketimine functionalities of both **5-^{t}Bu** and **5-Ad** bend significantly out of the CN_3 plane (**5-^{t}Bu**: C_{ket}−N3−C1 = 138.4(2)°; **5-Ad**: C_{ket}−N3−C1 = 125.0(1)°) (Figure 2 and Scheme 4), which breaks the C_2 symmetry of the monomeric unit. The discrepancies between the structural and the NMR spectral data can be reconciled by invoking fluxional solution-phase behavior. It can be imagined that, in solution, the ketimine "tail" is not fixed but wags or rotates rapidly, on the NMR time scale, along the N3−C1 bond, thus providing pseudo-C_2 symmetry in the spectra. Alternatively, π-conjugation of the *N*-ketimine lone pair into the CN_3 core or combined contributions from resonance forms **F** and **D**/**E** (Scheme 2) also explain the spectral features observed in solution.

Structural Comparison and Analyses. Molecular structure analyses were performed on **5-^{t}Bu**, **5-Ad**, **6**, and **7** to assess the structural and electronic impact, if any, of the ketimine substituents on the [{(X)C(NDipp)$_2$}FeBr]$_2$ framework. Any iminium-diamido resonance contributions in **5-^{t}Bu**, **5-Ad**, and **6** (Schemes 1 and 2) would be expected to manifest themselves most notably within the metrics of the XCN_2 ligand core when compared to resonance-limited **7**. For instance, the presence of diamido character in **5-^{t}Bu**, **5-Ad**, or **6** should result in longer C1−N_{Dipp} bonds (Scheme 4) than those of **7**.

At first glance, the average C1−N_{Dipp} bonds of **5-^{t}Bu**, **5-Ad**, **6**, and **7**, found in Scheme 4, appear to follow the trend **6** (1.355 Å) > **5-^{t}Bu** (1.345 Å) ≈ **7** (1.344 Å) > **5-Ad** (1.337 Å), suggesting the greatest resonance effects in **6**, modest resonance participation from the ^{t}Bu$_2$C═N- group of **5-^{t}Bu**, and negligible influence of the Ad═N substituent in **5-Ad**. Yet, the metrical parameters fail the 3σ-criterion, rendering the differences in the bond lengths statistically insignificant. Similarly, the relative Fe−N_{Dipp} bond distances, which would be anticipated to decrease upon greater ligand diamido resonance character, all fall within the statistical uncertainty of the measurement, precluding any meaningful Fe−N_{Dipp} bond assessment.

Nonetheless, *N*-amine π-contributions to the CN_3 ligand core of **6** are clearly evident from its solid-state structure (Figure 1). The backbone amine nitrogen of **6** adopts a planar geometry with a bond sum angle of $\sum_{N3}$ = 360° (Scheme 4), indicative of N(sp^2) hybridization. Consistent with this, the N3−C1 bond length of 1.380(2) Å in **6** is close to the 1.355 Å distance expected for an C(sp^2)−N(sp^2)R_2 bond and shorter than the 1.416 Å anticipated for a C(sp^2)−N(sp^3)R_2 bond.[25] These metrics reveal a detectable contribution from its iminium-diamido resonance form **C** (Scheme 1) and validates **6** as a suitable benchmark in which to compare **5-^{t}Bu** and **5-Ad**.

Initially, the notably bent ketimine backbones of **5-^{t}Bu** and **5-Ad** (Figure 2 and Scheme 4) appear to discount any *N*-ketimine π-participation into the CN_3 ligand core. Yet, upon closer examination of **5-^{t}Bu**, subtle but potentially significant structural features are revealed, which calls this into question. The C_{ket}−N3−C1 = 138.4(2)° bond angle of **5-^{t}Bu** deviates considerably from the 120° angle expected for a non-π-donating ketimine substituent, while the N3−C1 = 1.369(2) Å

DOI: 10.1021/acs.inorgchem.5b01815
Inorg. Chem. 2015, 54, 10030−10041

Scheme 4. Selected Bond Distances (Å) and Angles (deg) for 5-^{t}Bu, 5-Ad, 6, and 7[24]

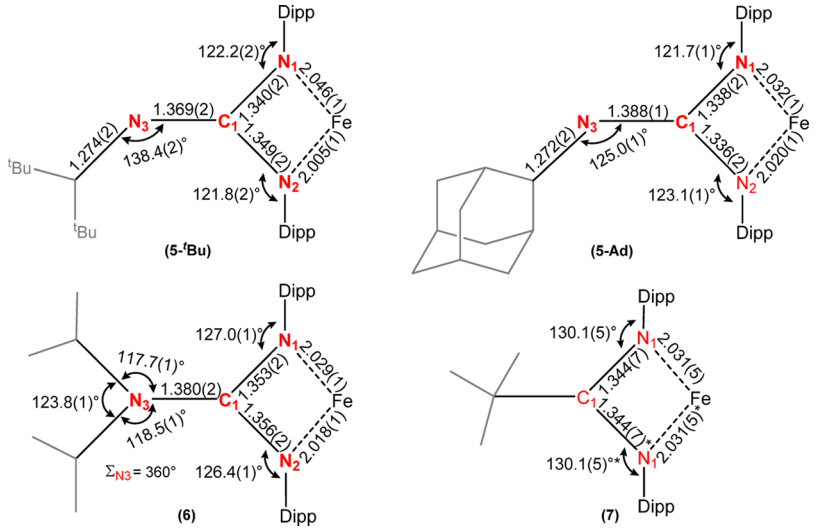

bond length is shorter than the 1.376 Å distance of a typical C(sp^2)−N(sp^2)R bond.[25] Moreover, these metrics compare favorably to those found for the −N═C^{t}Bu$_2$ moiety in polyunsaturated 8-(di-*tert*-butyl)-1-oxa-3,5,7-triaza-1,3,5,7-octatetraene, wherein the analogous C$_{ket}$−N−C bond angle (140.9(2)°) and N$_{ket}$−C bond distance (1.365(3) Å) are described as belonging to a weakly conjugated system.[26] In all, this suggests that the −N═C^{t}Bu$_2$ fragment may be expressing partial delocalization of the *N*-ketimine lone pair into the CN_3 core. On the other hand, the observed bond parameters may simply be an artifact of steric clashing between the bulky −N═C^{t}Bu$_2$ and Dipp groups, as marked by the pronounced twisting of the peripheral Dipp rings in **5-^{t}Bu** (vide infra).

Comparison of **5-^{t}Bu** to **5-Ad**, with its sterically less encumbering adamantyl imine backbone, shows a number of key differences between the complexes. In **5-Ad**, the C$_{ket}$−N3−C1 = 125.0(1)° bond angle (Figure 2 and Scheme 4) is unexceptional and in accord with that of an sp^2-hydridized nitrogen atom. Additionally, the N3−C1 = 1.388(1) Å bond length is fully in line with a C(sp^2)−N(sp^2)R single bond.[25] When compared structurally to the −N═Ad-containing oligonitrile (C$_6$H$_{10}$)N═C(^{t}Bu)N═C(Ph)-N═Ad, its relevant C$_{ket}$−N−C = 123.5(5)° and N$_{ket}$−C = 1.392(6) Å metrics closely match.[27] Showing that the −N═Ad group is not subjected to any considerable steric effects, comparison to the smaller dimethyl ketimine-functionalized guanidinate [(Me$_2$C═N)C(N^{i}Pr$_2$)$_2$]$^-$ (C$_{ket}$−N−C = 125.3(5)° and N$_{ket}$−C = 1.381(6) Å) shows nearly equivalent structural features.[20] These structural parameters clearly indicate that, in the solid state, no appreciable *N*-adamantyl π-participation is observed for **5-Ad** and, importantly, suggests that the contrasting features observed for **5-^{t}Bu** are likely of steric origin rather than electronic.

Among the solid-state structures of **5-^{t}Bu**, **5-Ad**, **6**, and **7**, the ketimine-guanidinates **5** are further differentiated, in part, by their peripheral ring angles. As shown in Scheme 4, the C1−N$_{Dipp}$−C$_{Dipp}$ angles in **5-^{t}Bu** (C1−N$_{Dipp}$−C$_{Dipp}$ = 122.0° (av)) and **5-Ad** (C1−N$_{Dipp}$−C$_{Dipp}$ = 122.4° (av)) are slightly more acute than those found for **6** (C1−N$_{Dipp}$−C$_{Dipp}$ = 126.7° (av)) and noticeably smaller than **7** (C1−N$_{Dipp}$−C$_{Dipp}$ = 130.1(5)°). These differences, albeit small, are important from the perspective that these angles relate to the projection of the electron lone pairs of the chelating N atoms, the directionality of which can have a dramatic effect on the chemistry of a metal.[17,28] Furthermore, the identity of the backbone substituent markedly influences the twist angle of the Dipp rings (with respect to the CN_3 plane), a phenomenon that largely appears to be of steric origin. For instance, in **7**, the amidinate ^{t}Bu backbone points away from the Dipp groups, allowing the pendant rings to adopt a nearly orthogonal orientation, as shown by the dihedral angles (87.5° and 89.6°) between the Dipp ring and CN_3 mean planes. As the bulk of the backbone group increases, i.e., **5-^{t}Bu** (59.8° and 72.9°) > **5-Ad** (68.8° and 72.8°) > **6** (78.41° and 81.0°), so does the slant of the ring angle. Indeed, this can be easily seen in the solid-state structure of **5-^{t}Bu** (Figure 2), with its Dipp rings conspicuously skewing away from one neighboring *tert*-butyl group of the −N═C^{t}Bu$_2$ backbone.

In summary, the comparative solid-state structural analysis of **5-^{t}Bu**, **5-Ad**, **6**, and **7** shows that the ketimine-guanidinates **5** are steric, but not electronic, standouts. In contrast to **6** and **7**, the pendant Dipp groups of both **5-^{t}Bu** and **5-Ad** must swing to avoid clashes with their inward bent ketimine substituents. When directly compared to **6**, which exhibits some quantifiable iminium-diamido resonance character in its structure, **5-Ad** shows no meaningful *N*-ketimine π-effects in its ligand architecture. For **5-^{t}Bu**, *N*-ketimine π-contributions to the ligand CN_3 core are not as clear-cut from its structural parameters, owing to potential steric effects, necessitating other characterization methods with which to gauge the electronic influence of the − N═C^{t}Bu$_2$ group.

Electronic Absorption Spectroscopy. To further probe for potential electronic contributions from the ketimine substituents of **5**, the solution-phase UV−vis absorption spectra, in THF, were collected for **5-^{t}Bu**, **5-Ad**, **6**, and **7**. It would be expected that if **5-^{t}Bu** or **5-Ad** were to express any *N*-ketimine resonance participation with the CN_3 ligand core, to access canonical forms **F** and **G** (Scheme 2), their electronic ligand environment on iron would approximate that of **6**, leading to similar absorption spectra. Instead, qualitatively by inspection, the iron complexes **5-^{t}Bu**, **5-Ad**, and **7** possess near identical light-yellow-colored solutions when compared in approximately equimolar concentrations. This observation is substantiated by their absorption spectra (Figure 3), as the λ_{max}

DOI: 10.1021/acs.inorgchem.5b01815
Inorg. Chem. 2015, 54, 10030−10041

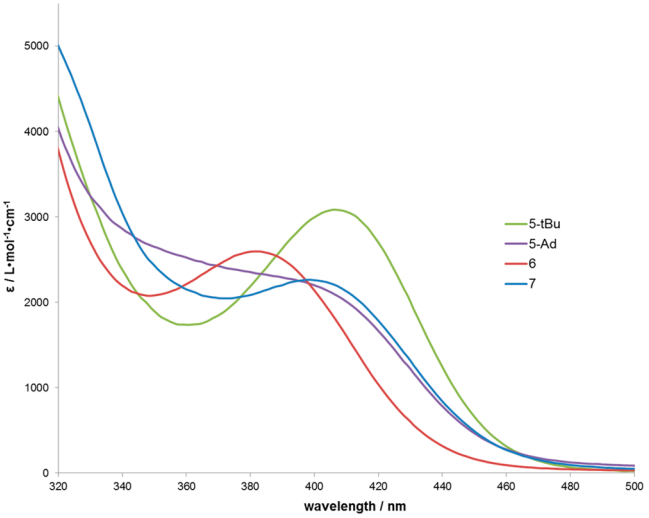

Figure 3. Room-temperature UV−vis absorption spectra for **5-^{t}Bu** (0.09 mM), **5-Ad** (0.12 mM), **6** (0.15 mM), and **7** (0.11 mM) in THF.

values of 402, 390, and 395 nm for **5-^{t}Bu**, **5-Ad**, and **7**, respectively, all closely fall within the same range. In contrast, **6** appears as a darker brown color by eye in solution and is distinguished by a ca. 20 nm blue shift in its UV−vis spectrum (Figure 3) as compared to **5-^{t}Bu**, **5-Ad**, and **7**. From this electronic absorption data, it can be stated that the ligand electronic structure of **5-^{t}Bu** and **5-Ad** is akin to that provided for iron by the amidinate ligand in **7**; that is, the ketimine backbone does not appear to provide any overt electronic contributions to the ligand manifold.

Electrochemistry. As a final measure of the electronic effects of appending a ketimine to a guanidinate framework, the solution-phase redox properties of **5-^{t}Bu**, **5-Ad**, **6**, and **7** were investigated by cyclic voltammetry. The cyclic voltammograms (CV) of all four complexes, in THF with $[NBu_4][PF_6]$ as supporting electrolyte, are qualitatively similar, each displaying electrochemically irreversible oxidation and reduction features at ca. 0 and −3.0 V (vs $Fc^{0/+}$), respectively. (N.B. **5-^{t}Bu** is the only complex that displays two distinct irreversible reduction features at ca. −3.0 and −3.5 V; see Figure S40 in the SI.) In between these terminal redox waves, the complexes all exhibit a semireversible Fe(II)/Fe(III) redox couple in their CVs that shows improved reversibility at higher scan rates (see the SI). Not surprisingly, **6** possesses the lowest Fe(II)/Fe(III) oxidation potential ($E_{1/2}$ = −0.45 V vs $Fc^{0/+}$) among the series, consistent with a more electron-rich iron metal center, reaffirming the superior electron-donating abilities of guanidinates over amidinate ligands like that in **7** (vide supra). For the remainder of the series, based upon the UV−vis absorption data, it would be predicted that the Fe(II)/Fe(III) redox values of **5-^{t}Bu**, **5-Ad**, and **7** should be comparable to one another; however, small but meaningful differences are observed. The oxidation potential of **5-^{t}Bu** ($E_{1/2}$ = −0.42 V vs $Fc^{0/+}$) is less than that of **7** ($E_{1/2}$ = −0.40 V vs $Fc^{0/+}$) and a notable 400 mV lower than **5-Ad** ($E_{1/2}$ = −0.38 V vs $Fc^{0/+}$). Placed within the context of its structural data, some delocalization of the *N*-ketimine lone pair into the CN_3 ligand core of **5-^{t}Bu** may be occurring, thus enhancing the donor strength of its ligand over those in **5-Ad** and **7**, the former of which exhibits no structural evidence of any *N*-ketimine π-conjugation (vide supra). An alternative and equally reasonable explanation is that inductive effects from the electron-donating *tert*-butyl groups of the ^{t}Bu$_2$C═N− moiety in **5-^{t}Bu** act to augment the donating abilities of its ketimine-guanidinate. Of course, a combination of conjugation and inductive effects may also serve to boost the relative electron-richness of the ligand framework in **5-^{t}Bu**.

Reactivity Studies. To conclude our comparative analysis, some preliminary reactivity studies were performed. As **7** has been shown to be able to effectively bind N_2 upon reduction in aromatic solvents to give the Fe(I) complex $[\{\kappa^1$-(^{t}Bu)C(NDipp)(η^6-NDipp)$\}$Fe(μ-N_2)$]_2$ (**8**),[24] we were interested in exploring the respective reduction chemistry of **5-^{t}Bu**, **5-Ad**, and **6**.

While it has been reported that attempts to reduce **6-Cl** were unsuccessful,[24] we found that treatment of **6** with excess magnesium in a 10:1 toluene/THF mixture under an N_2 atmosphere gives a deep red solution after 72 h, from which the Fe(I) toluene-capped complex $[(^i$NPr$_2)C$(NDipp$)_2]$Fe(η^6-C_7H_8) (**9**) can be isolated in good yield (Scheme 5). Attempts to reduce **6** in the absence of aromatic solvents provided only complex product mixtures. Interestingly, the related Fe(I) amidinate $[(^t$Bu$)C$(NDipp$)_2]$Fe(η^6-C_7H_8) (**10**) is also known but only forms upon the reduction of **7** in toluene under the strict exclusion of N_2.[24] At this time, the reason for the difference in N_2 binding preferences between **8** and **9** is not known.

Compound **9** can be isolated as dark red blocks from the storage of a saturated hexanes solution stored at −25 °C for 2 days and crystallizes in the triclinic space group $P\bar{1}$ with two, full independent molecules in its asymmetric unit. The metrical parameters of the two molecules are similar, and the solid-state structure of one is presented in Figure 4. Overall, the structure of **9** is unremarkable, especially as the coordination environment of its iron center is identical to that found in **10**. For instance, the iron−toluene Fe1−centroid distance (1.56 Å) of **9** is undistinguished from the corresponding bond length in **10** (1.564(3) Å).[24] Moreover, the metrical parameters of the CN_3 guanidinate core in **9** (C1−N1 = 1.338(4) Å; C1−N2 =

Scheme 5. Synthesis of 9, 10, and 11

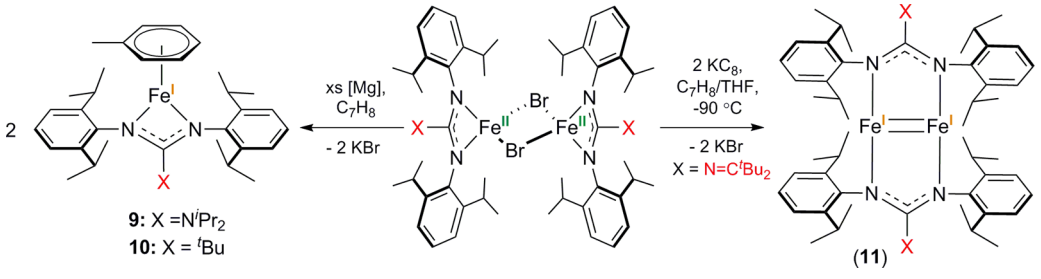

DOI: 10.1021/acs.inorgchem.5b01815
Inorg. Chem. 2015, 54, 10030−10041

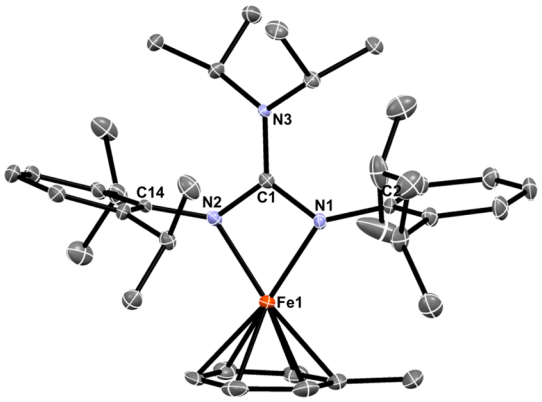

Figure 4. ORTEP diagram of **9** with 35% probability thermal ellipsoids. One of the two independent molecules is shown. Hydrogen atoms are omitted for clarity.

1.354(4) Å; C1−N3 = 1.389(4) Å; $\sum_{N3}$ = 360°) remain little changed as compared to **6** (Figure 1).

In contrast, the reduction chemistry of **5-^{t}Bu** and **5-Ad** differ substantially from that of **6** and **7**. Reduction of **5-Ad** with various reagents under varying conditions failed to give any tractable products. However, treatment of **5-^{t}Bu** with excess magnesium in a 20:1 toluene/THF mixture at room temperature for 3 days gives a deep red solution, from which red material can be isolated in low yield. The crude red solid is soluble in aliphatic and aromatic solvents, and its ^{1}H NMR spectrum displays five broad peaks ranging from 20.2 to −33.9 ppm.

X-ray crystallographic analysis of the red reduction product revealed the formation of the Fe(I)−Fe(I) complex [{μ-(^{t}Bu$_2$C═N)*C*(NDipp)$_2$}$_2$Fe$_2$] (**11**) (Figure 5). Complex **11**

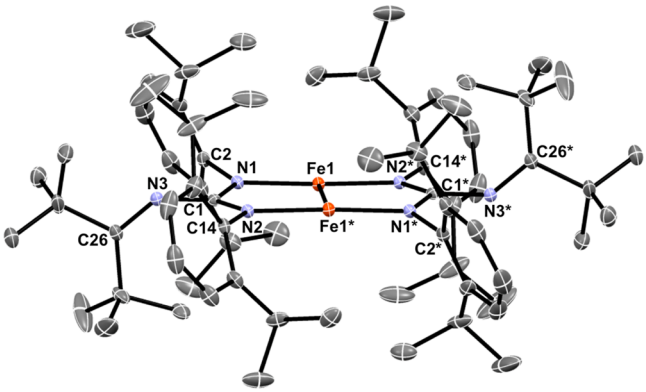

Figure 5. ORTEP diagram of **11**·C_7H_8 with 30% probability thermal ellipsoids. Hydrogen atoms and cocrystallized molecule of toluene are omitted for clarity.

cocrystallizes with one molecule of toluene in the monoclinic space group $P2_1/n$, and its solid-state molecular structure is shown in Figure 5. Quite notably, in **11**·C_7H_8, the ligation mode of the ketimine-guanidinate changes from an *N,N′*-chelate to a bridging ligand that accommodates two iron centers with T-shape geometry, each related by crystallographic inversion symmetry. Examination of the ligand framework, especially its CN_3 core, shows that the −N═C^{t}Bu$_2$ group remains bent (C_{ket}−N3−C1 = 137.9(2)°) with no statistical change in the N3−C1 = 1.380(3) Å bond length as compared to **5-^{t}Bu** (Scheme 4). Similarly, the peripheral aryl rings remain relatively tilted at 65.8° and 70.6°, as defined by the dihedral angle between the Dipp ring and CN_3 mean planes.

By far, the most salient feature of **11** is its Fe−Fe bonding interaction, which is exceedingly short at Fe1−Fe1* = 2.1516(5) Å. To the best of our knowledge, only one other iron−iron complex with a shorter metallic bond is known, namely, the closely related guanidinate complex [{μ-(*cis*-2,6-Me$_2$NC$_5$H$_8$)*C*(NDipp)$_2$}$_2$Fe$_2$] (**12**), with its Fe(I)−Fe(I) distance of 2.1270(7) Å reported by Jones and co-workers.[29] Upon the basis of their thorough electronic analysis of **12** and its high similarity to **11**, the short iron−iron distance in **11** is consistent with a formal Fe═Fe bond. Attempts to measure the room-temperature solution-phase magnetic moment of **11** by Evans' method, to compare to that recorded for **12** (8.1 μ_B, C_6D_6), were hampered by the limited solubility of pure, crystalline samples of **11**.[30]

When switching from magnesium to KC_8 as the reducing agent, **11** can be synthesized cleanly and in good yield (Scheme 5). It should be noted that **12** is the reduction product formed in the absence of aromatic solvents; however, when the analogous reduction is carried out in toluene, the mononuclear Fe(I) arene-capped complex [(*cis*-2,6-Me$_2$NC$_5$H$_8$)-*C*(NDipp)$_2$]Fe(η^6-C_7H_8) (**13**) is the sole product isolated in low yield.[31] Importantly, we have found that **11** is the only iron-containing product from the reduction of **5-^{t}Bu** regardless of whether aromatics are present or not. Moreover, we have observed no reaction of **11** with aromatic solvents at room temperature, while toluene solutions of **11** can be stored indefinitely when kept at −25 °C.

Finally, we sought to synthesize the Fe(I) carbonyl complex [(^{t}Bu$_2$C═N)*C*(NDipp)$_2$]Fe(CO)$_3$ (**14**) to examine its features in comparison to the previously reported carbonyl compounds [(X)*C*(NDipp)$_2$]Fe(CO)$_3$ (X = ^{t}Bu (**15**), *cis*-2,6-Me$_2$NC$_5$H$_8$ (**16**)).[29,31] Treatment of **5-^{t}Bu** with excess magnesium (or other reducing agents) in THF, toluene/THF, or other solvent combinations under a CO atmosphere resulted in the formation of intermediate dark green solutions that, upon standing for several minutes, redden, from which no tractable products are isolated. Similarly, addition of CO to **11** generates deep red-green solutions of complex product mixtures that fail to give **14**. The recalcitrance of **5-^{t}Bu** to form CO derivatives such as **14** is not understood but further exemplifies the differing reactivity of the ketimine-guanidinate complex from its iron amidinate and guanidinate counterparts.

SUMMARY

In an effort to further enhance the electron-richness of guanidinates, we engineered a new amidoimine ligand subclass featuring ketimines as backbone substituents. Unto themselves, monoanionic ketimides (e.g., ^{t}Bu$_2$C═N$^-$) are exemplary σ- and π-electron donors that often engage metals in linear C_{ket}−N−M bonding interactions.[18,19] We reasoned that by appending a ketimine onto a guanidinate-type platform, these electronic attributes, if successfully expressed, would give access to "ketimine-guanidinates" with competent donor abilities exceeding those of their guanidinate and amidinate counterparts.

To test this hypothesis, a comparative study across the series [(X)*C*(NDipp)$_2$}FeBr]$_2$ (X = N═C^{t}Bu$_2$ (**5-^{t}Bu**), N═Ad (**5-Ad**), N^{i}Pr$_2$ (**6**), ^{t}Bu (**7**)), differing only in their backbone, was performed. Structural and electronic analyses of **5-^{t}Bu**, **5-Ad**, **6**, and **7**, taken in whole, indicate that the ketimine groups impart no significant effect on the ligand electronic structure with the

DOI: 10.1021/acs.inorgchem.5b01815
Inorg. Chem. 2015, 54, 10030−10041

one exception that the ketimine-guanidinate ligand in **5-^{t}Bu** was shown electrochemically to be only a slightly weaker donor than the guanidinate in **6**. However, as a consequence of their geometric features, the ketimine-guanidinates are steric standouts. The inward-bending ketimine backbones in **5-^{t}Bu** and **5-Ad** clearly clash with the peripheral *N*Dipp groups of the ligand framework, noticeably tilting these rings toward the complexed iron centers. Interestingly, in broader comparison, **5-^{t}Bu** and **5-Ad** were also found to differ in their reduction chemistry. In particular, the reduction of **5-^{t}Bu** fails to give an arene or N_2-ligated Fe(I) complex, as compared to the reduction products of **6** and **7**, but rather gives the Fe(I)−Fe(I) dimer **11**, with a very short Fe═Fe double bond.

While ketimine substituents seemingly have little impact on the electronics of a guanidinate-type ligand, making ketimine-guanidinates more electronically akin to amidinates, ketimines are highly modular and easily made. Thus, as backbones, these groups add further synthetic versatility. Moreover, as we have shown, ketimines can augment the steric properties of amidoimine ligands. We intend to further investigate the distinctive chemistry our ketimine-guanidinate ligands, namely, $[(^tBu_2C{=}N)C(NDipp)_2]^-$, as it pertains to iron and other metal systems.

EXPERIMENTAL SECTION

General Considerations. All air- and moisture-sensitive operations were performed in an M. Braun drybox under an atmosphere of purified nitrogen or using high-vacuum standard Schlenk techniques. Diethyl ether, hexanes, pentanes, toluene, and THF were dried using a Pure Process Technology Solvent Purification System and subsequently stored under a dinitrogen atmosphere over activated 4 Å molecular sieves. All deuterated solvents were purchased from Cambridge Isotope Laboratories Inc., degassed by three freeze−pump−thaw cycles, and dried over activated 4 Å molecular sieves for 24 h prior to use. Celite, alumina, and 4 Å molecular sieves were heated to 150 °C for at least 24 h and then cooled under vacuum. LiN═C^{t}Bu$_2$,[32] LiN═Ad,[33] anhydrous lutidinium chloride,[34] DippN═C═NDipp,[35] [(^{i}Pr$_2$N)*C*(NDipp)$_2$]K,[23] and [{(^{t}Bu)*C*(NDipp)$_2$}FeBr]$_2$ (**7**)[24] were prepared following literature procedures, while all other reagents were purchased from commercial suppliers and used as received. (^{t}Bu)*C*(NDipp)(NHDipp) was prepared by treating DippN═C═NDipp with 1 equiv of ^{t}BuLi in Et$_2$O followed by aqueous workup,[36] and [(^{t}Bu)*C*(NDipp)$_2$]K was prepared by treating (^{t}Bu)*C*(NDipp)(NHDipp) with KH in THF.[24] NMR spectra were recorded on a JEOL ECA 600 MHz, a Bruker AVANCE III 400 MHz, or a Bruker DPX 300 MHz spectrometer. ^{1}H NMR and ^{13}C NMR spectra are referenced to SiMe$_4$ using the residual ^{1}H solvent peaks as internal standards or the characteristic ^{13}C resonances of the solvent. ^{7}Li{^{1}H} spectra were referenced to external LiCl in D$_2$O. IR data were collected using a Thermo Scientific Nicolet iS5 spectrometer. The intensities are reported relative to the most intense peak and are given in parentheses using the following abbreviations: w = weak, m = medium, s = strong. UV−vis spectra were recorded on a Shimadzu UV-3101PC UV−vis/NIR scanning spectrophotometer. Elemental analyses were performed by Robertson Microlit Laboratories, Inc. and Midwest Microlab, LLC.

Synthesis of [(^{t}Bu$_2$C═N)*C*(NDipp)$_2$]Li(THF)$_2$ (1-^{t}Bu). To a 100 mL Cajon flask equipped with a small stir bar were added DippN═C═NDipp (8.79 g, 24.2 mmol), ^{t}Bu$_2$C═NLi (3.58 g, 24.3 mmol), and THF (40 mL). The reaction mixture was stirred at 65 °C for 1 day. Subsequently, the volatiles were removed under reduced pressure to afford an off-white powder, which was purified by crystallization from a hexane/THF (10:1) solution stored at −25 °C for 2 days, giving the product as a white, crystalline solid. Yield: 13.1 g, 83%. ^{1}H NMR (25 °C, 400 MHz, C$_6$D$_6$): δ 1.03 (s, 18H, N═C^t*Bu*$_2$), 1.28 (d, 12H, J_{HH} = 8 Hz, CH*Me*$_2$), 1.37 (t, 8H, J_{HH} = 8 Hz, THF), 1.52 (d, 12H, J_{HH} = 8 Hz, CH*Me*$_2$), 3.55 (t, 8H, J_{HH} = 8 Hz, THF), 4.07 (sept, 4H, J_{HH} = 8 Hz, C*H*Me$_2$), 7.05 (t, 2H, J_{HH} = 8 Hz, *p*-Ar*H*), 7.22 (d, 4H, J_{HH} = 8 Hz, *m*-Ar*H*). ^{13}C{^{1}H} NMR (25 °C, 100 MHz, C$_6$D$_6$): δ 22.2 (CH*Me*$_2$), 25.4 (THF), 25.7 (CH*Me*$_2$), 28.6 (N═C^t*Bu*$_2$), 30.5 (N═C^t*Bu*$_2$), 43.5 (*C*HMe$_2$), 68.4 (THF), 120.8 (aryl), 122.4 (aryl), 142.3 (aryl), 147.8(aryl), 161.1 (N═C^{t}Bu$_2$), 172.3 (N$_3$*C*). ^{7}Li{^{1}H} NMR (25 °C, 155 MHz, C$_6$D$_6$): δ 1.6. IR (KBr pellet cm^{-1}): 3424 (w), 3053 (m), 3010 (s), 2964 (s), 2934 (s), 2870 (s), 1891 (w), 1829 (w), 1771 (w), 1655 (s), 1611 (w), 1581 (w), 1450 (s), 1423 (s), 1388 (s), 1374 (s), 1364 (s), 1317 (s), 1242 (s), 1205 (m), 1189 (m), 1174 (m), 1156 (w), 1142 (w), 1110 (m), 1091 (m), 1045 (s), 972 (m), 930 (m), 892 (m), 885 (m), 804 (w), 786 (m), 765 (w), 750 (s), 723 (w), 683 (w), 668 (m), 627 (w), 573 (w), 541 (w), 512 (w). Anal. Calcd for $C_{42}H_{68}LiN_3O_2$: C, 77.14; H, 10.48; N, 6.43. Found: C, 76.84; H, 9.97; N, 6.49.

Synthesis of [(Ad═N)*C*(NDipp)$_2$]Li(THF)$_2$ (1-Ad). To a 50 mL Cajon flask equipped with a small stir bar were added DippN═C═NDipp (1.91 g, 5.3 mmol), LiN═Ad (840 mg, 5.4 mmol), and THF (20 mL). The reaction mixture was stirred at 65 °C for 1 day. Subsequently, the volatiles were removed under reduced pressure to afford an off-white powder, which was purified by crystallization from a toluene/THF (10:1) solution stored at −25 °C for 2 days, giving the product as a white, crystalline solid. Yield: 2.1 g, 77%. ^{1}H NMR (25 °C, 400 MHz, C$_6$D$_6$/THF-d_8 (10:1)): δ 1.18 (d, J_{HH} = 6 Hz, 18H), 1.46−1.49 (m, 17H), 1.48 (m, 8H), 2.16 (s, 1H, Ad*H*), 2.38 (br s, 2H, Ad*H*), 3.85 (br m, 4H, C*H*Me$_2$), 6.93 (m, 2H, Ar*H*), 7.03−7.20 (br m, 4H, Ar*H*). ^{1}H NMR (−50 °C, 600 MHz, C$_7$D$_8$) (major isomer): δ 1.28 (d, J_{HH} = 6 Hz), 1.36 (d, J_{HH} = 6 Hz), 1.39, 1.43, 1.47, 1.49 (d, J_{HH} = 6 Hz), 1.52, 1.57, 1.59, 1.69, 1.71, 1.80 (d, J_{HH} = 6 Hz), 2.46 (s), 2.51 (s), 2.70 (s), 3.71 (br s, THF), 3.90 (sept, J_{HH} = 6 Hz, 2H, C*H*Me$_2$), 4.17 (sept, J_{HH} = 6 Hz, 2H, C*H*Me$_2$), 7.13 (s, Ar*H*), 7.14 (s, Ar*H*), 7.15 (s, Ar*H*), 7.21 (d, J_{HH} = 6 Hz, 2H, ArH), 7.33 (d, J_{HH} = 6 Hz, 2H, Ar*H*). ^{1}H NMR (50 °C, 600 MHz, C$_7$D$_8$): δ 1.15 (br s), 1.22 (br m), 1.44 (s), 1.50 (s), 1.53 (s), 1.63 (s), 2.33 (br s), 3.53 (s, THF), 3.85 (br s), 6.97 (s), 7.09 (s). ^{7}Li{^{1}H} NMR (25 °C, 155 MHz, C$_6$D$_6$): δ −0.9 (minor isomer), 2.73 (major isomer). IR (KBr pellet, cm^{-1}): 3051 (w), 2956 (s), 2915 (s), 2858 (s), 1710 (s), 1678 (s), 1628 (w), 1584 (w), 1460 (s), 1429 (s), 1397 (m), 1376 (m), 1352 (m), 1316 (s), 1254 (m), 1235 (m), 1203 (m), 1188 (w), 1142 (w), 1106 (w), 1098 (w), 1063 (m), 1051 (m), 1002 (w), 950 (m), 932 (w), 892 (m), 832 (w), 784 (m), 768 (w), 748 (m), 695 (w), 607 (w), 499 (m), 412 (w). Anal. Calcd for $C_{43}H_{64}LiN_3O$: C, 78.02; H, 9.75; N, 6.35. Anal. Calcd for $C_{43}H_{64}LiN_3O_2{\cdot}C_6H_{14}$: C, 78.67; H, 10.51; N, 5.62. Found: C, 79.03; H, 9.83; N, 6.06.

Synthesis of (NH$_2$)*C*(NDipp)(NHDipp) (2). To a 20 mL scintillation vial containing a small stir bar were added **1-^{t}Bu** (100 mg, 0.15 mmol) and Et$_2$O (5 mL). To this was added two drops of distilled water, and the solution was stirred at 25 °C for 1 h. The colorless solution was dried over anhydrous MgSO$_4$ and subsequently filtered through Celite. Et$_2$O was removed under reduced pressure, giving a colorless solid. A pure crystalline, white solid of **2** was obtained from a concentrated benzene solution layered with hexane. Yield: 40 mg, 72%. ^{1}H NMR (25 °C, 600 MHz, C$_6$D$_6$): δ 0.43 (s), 1.06 (br s), 1.22 (d, J_{HH} = 6 Hz), 3.01 (s, 2H, N*H*$_2$), 3.50 (br s, 4H, C*H*Me$_2$), 7.08 (s, 6H, Ar*H*), 10.94 (br s, 1H, N*H*). ^{1}H NMR (−40 °C, 600 MHz, C$_7$D$_8$): δ 0.55 (d, 6H, J_{HH} = 6 Hz, CH*Me*$_2$), 1.12 (d, 6H, J_{HH} = 6 Hz, CH*Me*$_2$), 1.30 (d, 6H, J_{HH} = 6 Hz, CH*Me*$_2$), 1.48 (d, 6H, J_{HH} = 6 Hz, CH*Me*$_2$), 2.90 (s, 2H, N*H*$_2$), 3.29 (sept, 2H, J_{HH} = 6 Hz, C*H*Me$_2$), 3.62 (sept, 2H, J_{HH} = 6 Hz, C*H*Me$_2$), 7.09 (br s, 1H, Ar*H*), 7.12 (br s, 1H, Ar*H*), 7.14 (br m, 4H, Ar*H*), 11.81 (s, 1H, N*H*). IR (KBr pellet, cm^{-1}): 3504 (s, ν NH$_2$), 3398 (s, ν NH), 2959 (s), 2926 (s), 2866 (s), 1937 (w), 1871 (w), 1804 (w), 1652 (s), 1576 (s), 1463 (s), 1429 (s), 1382 (m), 1361 (m), 1323 (s), 1248 (s), 1204 (w), 1197 (m), 1178 (w), 1103 (m), 1075 (w), 1057 (w), 1044 (w), 987 (w), 936 (w), 885 (w), 835 (s), 800 (s), 777 (m), 754 (s), 709 (w), 678 (w), 640 (w), 596 (w), 539 (w), 511 (w), 433 (m). ESI-MS: *m*/*z* 380.34 ([M + H]$^+$; calcd *m*/*z* 380.31).

Synthesis of (^{t}Bu$_2$C═N)*C*(NDipp)(NHDipp) (3-^{t}Bu). To a 100 mL round-bottom flask equipped with a medium stir bar was added **1-^{t}Bu** (9.45 g, 14.4 mmol), lutidinium chloride (2.1 g, 14.6 mmol), and THF (50 mL). The colorless reaction mixture was stirred at room

DOI: 10.1021/acs.inorgchem.5b01815
Inorg. Chem. 2015, 54, 10030−10041

temperature under an inert atmosphere for 1 day and was subsequently filtered through Celite supported on a medium-porosity glass frit. The volatiles of the filtrate were removed in vacuo to afford a colorless semisolid. To this was added hexane (100 mL), and the solution was again filtered. Hexane was then removed under reduced pressure to afford **3-^{t}Bu** as white solid. Yield: 7.0 g, 96%. ^{1}H NMR (25 °C, 400 MHz, C_6D_6): δ 0.64 (s), 0.91 (br s), 1.09 (s), 1.25 (s), 1.34 (s), 1.43 (s), 3.54 (br s, C*H*Me$_2$), 3.63 (br s, C*H*Me$_2$), 4.88 (br s, N*H*, minor isomer), 5.46 (br s, N*H*, major isomer), 7.02 (br s, Ar*H*), 7.12 (br m, Ar*H*), 7.26 (br s, Ar*H*). ^{1}H NMR (−60 °C, 600 MHz, C_7D_8): δ 0.92 (d, 6H, J_{HH} = 12 Hz, CH*Me*$_2$, major isomer), 1.07 (s, 18H, N=C^t*Bu*$_2$, minor isomer), 1.15 (d, 6H, J_{HH} = 12 Hz, CH*Me*$_2$, minor isomer), 1.23 (s, 18H, N=C^t*Bu*$_2$, major isomer), 1.23 (6H, CH*Me*$_2$, minor isomer), 1.30 (d, 6H, J_{HH} = 12 Hz, CH*Me*$_2$, major isomer), 1.39 (d, 6H, J_{HH} = 6 Hz, CH*Me*$_2$, major isomer), 1.46 (d, 6H, J_{HH} = 6 Hz, CH*Me*$_2$, major isomer) 1.46 (6H, CH*Me*$_2$, minor isomer), 1.50 (d, 6H, J_{HH} = 6 Hz, CH*Me*$_2$, minor isomer), 3.57 (sept, 2H, J_{HH} = 6 Hz, C*H*Me$_2$, major isomer), 3.68 (sept, 2H, J_{HH} = 6 Hz, C*H*Me$_2$, major isomer), 3.68 (br, 2H, C*H*Me$_2$, minor isomer), 3.86 (br, 2H, C*H*Me$_2$, minor isomer), 4.79 (s, 1H, N*H*, minor isomer), 5.53 (s, 1H, N*H*, major isomer), 7.07−7.29 (m, Ar*H*, major and minor isomers). IR (KBr pellet, cm^{-1}): 3423 (s, ν NH), 3057 (m), 3016 (m), 2961 (s), 2868 (s), 1943 (w), 1664 (s), 1611 (s), 1581 (s), 1481 (s), 1460 (s), 1430 (s), 1366 (m), 1359 (s), 1324 (m), 1303 (w), 1276 (s), 1235 (s), 1218 (m), 1195 (m), 1173 (m), 1144 (m), 1109 (m), 1048 (m), 973 (m), 933 (w), 843 (m), 802 (m), 785 (m), 769 (s), 751 (m), 714 (m), 687 (w), 536 (w), 489 (w). ESI-MS: m/z 504.44 ([M + H]$^+$; calcd m/z 504.43).

Synthesis of (Ad=N)*C*(NDipp)(NHDipp) (3-Ad). To a 50 mL round-bottom flask equipped with a small stir bar were added **1-Ad** (2.5 g, 3.8 mmol) and diethyl ether (20 mL). To this solution was added distilled water (1 mL). The suspension was vigorously stirred for 1 h at room temperature. After 1 h, the suspension settled, the organic layer was extracted with CH_2Cl_2 (20 mL) and dried over $MgSO_4$, and the volatiles were removed under reduced pressure to afford a white solid. A pure crystalline, white solid of **3-Ad** was obtained from a concentrated hexane solution kept at −10 °C for 2 days. Yield: 1.8 g, 92%. ^{1}H NMR (25 °C, 600 MHz, C_7D_8): δ 0.83−0.97 (m), 1.10 (br s), 1.29 (d, J_{HH} = 6 Hz), 1.34 (br s), 1.41 (s), 1.44 (d, J_{HH} = 6 Hz), 1.52 (s), 1.56 (d, J_{HH} = 6 Hz), 1.63−1.69 (m), 2.42 (s), 2.46 (s), 2.51 (br s), 3.23 (s, C*H*Me$_2$), 3.49 (sept, J_{HH} = 6 Hz, C*H*Me$_2$), 3.49 (br s, C*H*Me$_2$), 3.59 (sept, J_{HH} = 6 Hz, C*H*Me$_2$), 5.07 (br s, 1H, N*H*, minor isomer), 5.49 (s, 1H, N*H*, major isomer), 7.10 (br s, Ar*H*), 7.24 (d, J_{HH} = 6 Hz, Ar*H*). ^{1}H NMR (−50 °C, 600 MHz, C_7D_8): δ 0.50 (d, J_{HH} = 6 Hz), 0.94 (d, J_{HH} = 6 Hz), 1.00 (d, J_{HH} = 12 Hz), 1.02 (br s), 1.14 (br d, J_{HH} = 6 Hz), 1.26 (br), 1.36 (t, J_{HH} = 6 Hz), 1.45 (br s), 1.47 (d, J_{HH} = 6 Hz), 1.51 (br), 1.53 (br), 1.58 (t, J_{HH} = 12 Hz), 1.65 (br d, J_{HH} = 12 Hz), 2.48 (br s, 2H, Ad*H*, major isomer), 2.48 (br s, 2H, Ad*H*, minor isomer), 2.52 (br s, 1H, Ad*H*, minor isomer), 2.57 (br s, 1H, Ad*H*, major isomer), 2.62 (br s, 1H, Ad*H*, major isomer), 3.17 (br s, 1H, Ad*H*, minor isomer), 3.31 (br sept, 1H, C*H*Me$_2$, major isomer), 3.44 (br sept, 1H, C*H*Me$_2$, major isomer), 3.52 (sept, 2H, J_{HH} = 6 Hz, C*H*Me$_2$, minor isomer), 3.57 (br sept, 1H, C*H*Me$_2$, major isomer), 3.65 (sept, 2H, J_{HH} = 6 Hz, C*H*Me$_2$, minor isomer), 3.80 (br sept, 1H, C*H*Me$_2$, major isomer), 5.20 (s, 1H, N*H*, major isomer), 5.56 (s, 1H, N*H*, minor isomer), 6.94−7.29 (m, Ar*H*, major and minor isomers). IR (KBr pellet, cm^{-1}): 3443 (w, ν NH), 3371 (w, ν NH), 3053 (w), 2959 (s), 2922 (s), 2855 (m), 1721 (m), 1664 (m), 1637 (s), 1584 (m), 1469 (m), 1451 (m), 1434 (m), 1380 (w), 1357 (w), 1331 (w), 1291 (w), 1252 (w), 1226 (m), 1191 (w), 1109 (w), 1073 (w), 1058 (w), 1000 (w), 953 (w), 936 (w), 883 (w), 845 (w), 804 (w), 790 (w), 766 (w), 750 (m), 720 (w), 691 (w), 668 (w), 618 (w), 571 (w), 466 (w), 447 (w), 425 (w). ESI-MS: m/z 512.41 ([M + H]$^+$; calcd m/z 512.40).

Synthesis of [(^{t}Bu$_2$C=N)*C*(NDipp)$_2$]K (4-^{t}Bu). To a 100 mL round-bottom flask equipped with a stir bar and fitted with a glass stopper were added **3-^{t}Bu** (7.0 g, 13.9 mmol), potassium hydride (695 mg, 17.4 mmol), and THF (50 mL). The glass stopper of the flask was periodically removed to release the evolved hydrogen gas. After 2 h, the solution was filtered through Celite supported on a medium-porosity glass frit to remove excess potassium hydride. All volatiles were removed under reduced pressure to afford a colorless semisolid. To this was added hexane (20 mL), and the semisolid triturated to obtain a white powder, which was subsequently dried under reduced pressure to afford **4-^{t}Bu** as a solvate-free white solid. Note: Crystals of **4-^{t}Bu** were grown from a THF/Et$_2$O mixture, giving the solvated complex [(^{t}Bu$_2$C=N)*C*(NDipp)$_2$]K(Et$_2$O)(THF) (see Figure S31). Yield: 7.4 g, 99%. ^{1}H NMR (25 °C, 400 MHz, C_6D_6/C_5D_5N (10:1)): δ 1.12 (d, 12H, J_{HH} = 8 Hz, CH*Me*$_2$), 1.24 (s, 18H, N=C^t*Bu*$_2$), 1.39 (d, 12H, J_{HH} = 8 Hz, CH*Me*$_2$), 4.16 (sept, 4H, J_{HH} = 8 Hz, C*H*Me$_2$), 6.91 (t, 2H, J_{HH} = 8 Hz, *p*-Ar*H*), 7.11 (d, 4H, J_{HH} = 8 Hz, *m*-Ar*H*). ^{13}C{^{1}H} NMR (25 °C, 100 MHz, C_6D_6/THF-d_8 (10:1)): δ 22.8 (CH*Me*$_2$), 24.9 (CH*Me*$_2$), 28.3 (N=C^t*Bu*$_2$) 30.8 (N=C^t*Bu*$_2$), 43.1 (CHMe$_2$), 118.7 (aryl), 121.9 (aryl), 142.0 (aryl), 156.8 (N=C^{t}Bu$_2$), 168.7 (N_3C), one aryl carbon was not observed. IR (KBr pellet, cm^{-1}): 3050 (w), 2959 (s), 2920 (m), 2869 (m), 1661 (m), 1611 (w), 1579 (w), 1456 (s), 1425 (s), 1350 (m), 1310 (m), 1232 (m), 1182 (m), 1110 (w), 1050 (w), 973 (w), 930 (w), 860 (w), 805 (w), 771 (m), 750 (m), 730 (w), 688 (w), 668 (w). Anal. Calcd for $C_{34}H_{52}KN_3$: C, 75.36; H, 9.67; N, 7.75. Found: C, 75.62; H, 9.90; N, 7.71.

Synthesis of [(Ad=N)*C*(NDipp)$_2$]K(THF)$_2$ (4-Ad). To a 50 mL round-bottom flask equipped with a small stir bar and fitted with a glass stopper were added **3-Ad** (2.0 g, 3.9 mmol), potassium hydride (200 mg, 5 mmol), and THF (20 mL). The glass stopper of the flask was periodically removed to release the evolved hydrogen gas. After 6 h, the solution was filtered through Celite supported on a medium-porosity glass frit to remove excess potassium hydride. All volatiles were removed under reduced pressure to afford a colorless semisolid. To this was added hexane (10 mL), and the semisolid triturated to obtain a white powder, which was subsequently dried under reduced pressure to afford **4-Ad** as a white solid. Yield: 2.0 g, 92%. ^{1}H NMR (25 °C, 400 MHz, C_6D_6/C_5D_5N (10:1)): δ 1.20 (s), 1.21 (s), 1.42 (s), 1.49 (s), 1.52 (s), 1.60 (s), 2.51 (br s, Ad*H*), 4.12 (br s, C*H*Me$_2$), 6.98 (t, 2H, J_{HH} = 8 Hz, *p*-Ar*H*), 7.18 (d, 4H, *m*-Ar*H*). IR (KBr pellet, cm^{-1}): 3054 (m), 2957 (s), 2913 (s), 2855 (s), 1667 (s), 1629 (m), 1584 (m), 1502 (s), 1426 (s), 1375 (s), 1369 (s), 1307 (s), 1239 (s), 1226 (s), 1188 (s), 1156 (w), 1142 (w), 1096 (m), 1071 (m), 1039 (w), 1000 (w), 971 (w), 947 (m), 889 (m), 855 (w), 845 (w), 805 (w), 775 (s), 766 (s), 751 (m), 727 (w), 694 (w), 628 (w), 569 (w), 464 (w), 422 (w). Anal. Calcd for $C_{43}H_{64}KN_3O_2$: C, 74.41; H, 9.29; N, 6.05. Anal. Calcd for $C_{43}H_{64}KN_3O_2{\cdot}C_6H_{14}$: C, 75.43; H, 10.08; N, 5.39. Found: C, 75.91; H, 9.34; N, 6.75.

Synthesis of [{(^{t}Bu$_2$C=N)*C*(NDipp)$_2$}FeBr]$_2$ (5-^{t}Bu). To a 250 mL round-bottom flask equipped with a stir bar were added $FeBr_2$ (3.0 g, 13.9 mmol) and THF (100 mL). The brown suspension was stirred for 1 h to dissolve most of the $FeBr_2$. To this brown solution was added slowly dropwise a THF (20 mL) solution of **4-^{t}Bu** (7.5 g, 13.9 mmol). An immediate color change to brown-gray with formation of insoluble gray particles was observed. The reaction mixture was stirred at room temperature for 36 h. Subsequently, the solution was filtered through Celite supported on a medium-porosity glass frit to remove most of the KBr. All volatiles were removed under reduced pressure to afford a yellow semisolid. To this was added hexane (25 mL), and the volatiles were removed under reduced pressure to afford a brown solid. To this was added toluene (75 mL), and the solution stirred for 1 h and again filtered. The filtrate was concentrated (ca. 10 mL) and kept at −25 °C for 2 days to afford brown-yellow crystals. Yield: 7.2 g, 81%. ^{1}H NMR (25 °C, 600 MHz, C_6D_6): δ −11.1 (s, 12H, CH*Me*$_2$), −10.7 (s, 2H, *p*-Ar*H*), 1.4 (s, 12H, CH*Me*$_2$), 9.5 (s, 18H, N=C^t*Bu*$_2$), 15.8 (br s, 4H), 21.8 (s, 4H). IR (KBr pellet, cm^{-1}): 3172 (w), 3060 (w), 2964 (s), 2869 (m), 1681)s), 1588 (w), 1577 (w), 1528 (w), 1485 (m), 1456 (s), 1432 (s), 1375 (s), 1362 (s), 1324 (s), 1272 (s), 1252 (m), 1216 (m), 1178 (w), 1108 (w), 1047 (m), 971 (m), 931 (w), 891 (m), 791 (s), 776 (m), 749 (s), 733 (w), 698 (w), 668 (w), 629 (w), 543 (w), 516 (w), 502 (w), 431 (w), 417 (w). μ_{eff} (Evans, C_6D_6, 298 K): 6.5 μ_B. Anal. Calcd $C_{68}H_{104}Br_2Fe_2N_6$: C, 63.95; H, 8.21; N, 6.58. Found: C, 63.68; H, 8.33; N, 6.37.

Synthesis of [{(Ad=N)*C*(NDipp)$_2$}FeBr]$_2$ (5-Ad). To a 20 mL scintillation vial containing a small stir bar was added $FeBr_2$ (268 mg, 1.2 mmol) and THF (10 mL). The brown suspension was stirred for 1

DOI: 10.1021/acs.inorgchem.5b01815
Inorg. Chem. 2015, 54, 10030−10041

Table 1. X-ray Crystallographic Data for 2, 3-^{t}Bu, 5-^{t}Bu, and 5-Ad·2C_7H_8, 6, 9, and 11

	2	3-^{t}Bu	5-^{t}Bu	5-Ad·2C_7H_8
empirical formula	$C_{25}H_{37}N_3$	$C_{34}H_{53}N_3$	$C_{68}H_{104}Br_2Fe_2N_6$	$C_{70}H_{96}Br_2Fe_2N_6·2C_7H_8$
cryst habit, color	block, colorless	block, colorless	plate, yellow	plate, yellow
cryst size (mm)	0.20 × 0.18 × 0.18	0.25 × 0.20 × 0.18	0.28 × 0.22 × 0.12	0.24 × 0.22 × 0.12
cryst syst	orthorhombic	orthorhombic	orthorhombic	monoclinic
space group	$C222_1$	*Pbca*	*Pbca*	$P2_1/c$
volume (Å^3)	4703.1(13)	6336.3(5)	6868.9(6)	3917.4(3)
a (Å)	14.409(2)	16.7641(8)	11.7487(6)	10.2631(4)
b (Å)	19.966(3)	18.7587(9)	18.2330(9)	12.9721(5)
c (Å)	16.347(3)	20.1491(9)	32.0658(16)	29.4875(12)
α (deg)	90	90	90	90
β (deg)	90	90	90	93.7510(10)
γ (deg)	90	90	90	90
Z	8	8	4	2
F_w (g/mol)	379.58	503.79	1277.09	1477.31
density (calcd) (Mg/m^3)	1.072	1.056	1.235	1.252
abs coeff (mm^{-1})	0.063	0.061	1.627	1.436
F_{000}	1664	2224	2704	1560
total no. of reflns	18 068	78 902	94 571	50 454
unique reflns	2221	6801	6289	10 114
final R indices [$I > 2\sigma(I)$]	R1 = 0.0653, wR2 = 0.1725	R1 = 0.0634, wR2 = 0.1892	R1 = 0.0296, wR2 = 0.0864	R1 = 0.0299, wR2 = 0.0726
largest diff peak and hole (e/Å^3)	0.660 and −0.320	0.648 and −0.297	0.458 and −0.386	0.482 and −0.349
GOF	1.040	1.217	1.079	1.020

	6	9	11·C_7H_8
empirical formula	$C_{62}H_{96}Br_2Fe_2N_6$	$C_{38}H_{56}FeN_3$	$C_{68}H_{104}Fe_2N_6·C_7H_8$
cryst habit, color	block, brown	plate, red	block, dark red
cryst size (mm)	0.3 × 0.28 × 0.25	0.20 × 0.16 × 0.10	0.24 × 0.21 × 0.19
cryst syst	triclinic	triclinic	monoclinic
space group	$P\bar{1}$	$P\bar{1}$	$P2_1/n$
volume (Å^3)	1606.10(19)	3440.7(5)	3509.3(4)
a (Å)	10.7050(7)	10.0431(9)	12.0199(8)
b (Å)	10.7315(8)	16.4487(15)	18.3752(13)
c (Å)	15.9169(11)	21.5381(18)	15.9526(11)
α (deg)	109.3010(10)	95.125(2)	90
β (deg)	95.0830(10)	102.729(2)	95.140(2)
γ (deg)	107.8040(10)	94.226(2)	90
Z	1	4	1
F_w (g/mol)	1196.96	610.70	2351.61
density (calcd) (Mg/m^3)	1.238	1.179	1.113
abs coeff (mm^{-1})	1.735	0.467	0.456
F_{000}	632	1324	1269
total no. of reflns	21 492	38 591	37 335
unique reflns	6269	9179	7442
final R indices [$I > 2\sigma(I)$]	R1 = 0.0269, wR2 = 0.0713	R1 = 0.0587, wR2 = 0.1874	R1 = 0.0641, wR2 = 0.1857
largest diff peak and hole (e/Å^3)	0.701 and −0.660	0.488 and −0.468	0.967 and −0.843
GOF	1.014	0.915	1.039

h to dissolve most of the $FeBr_2$. To this brown solution was added dropwise a THF (5 mL) solution of **4-Ad** (680 mg, 1.2 mmol). An immediate color change to pale yellow with a formation of insoluble gray particles was observed. The whole suspension was stirred at room temperature for 36 h. The suspension was filtered through Celite supported on a medium-porosity glass frit to remove most of the KBr. All volatiles were removed under reduced pressure to afford a brown-yellow semisolid. To this was added hexane (5 mL), and the volatiles were removed under reduced pressure to afford a brown-yellow solid. To this was added toluene (10 mL) to redissolve the material, and the solution was again filtered. The filtrate was concentrated (ca. 3 mL) and kept at −25 °C for 2 days to afford amber-yellow crystals. Yield: 560 mg, 72%. ^{1}H NMR (25 °C, 400 MHz, C_6D_6): δ −9.98 (s, 2H), −5.51 (s, 12H, CHMe_2), 0.31 (s, 2H), 3.30 (s, 4H), 4.04 (br s, 12H, CHMe_2), 4.86 (s, 4H), 6.07 (s, 4H), 7.19 (br s, 2H), 8.58 (br s, 2H), 21.10 (br s, 4H). IR (KBr pellet, cm^{-1}): 3215 (w), 3059 (w), 2961 (s), 2915 (s), 2857 (m), 1706 (m), 1685 (m), 1593 (m), 1550 (m), 1442 (s), 1415 (s), 1376 (m), 1351 (m), 1321 (m), 1251 (m), 1206 (w), 1177 (w), 1097 (m), 1070 (m), 953 (w), 934 (w), 901 (m), 882 (w), 796 (m), 749 (m), 720 (w), 697 (w), 593 (w), 568 (w), 520 (w), 467 (w), 446 (w), 422 (w). Anal. Calcd $C_{68}H_{104}Br_2Fe_2N_6$: C, 65.02; H, 7.48; N, 6.50. Found: C, 64.30; H, 7.25; N, 6.48.

Synthesis of [{(^{i}Pr$_2$N)C(NDipp)$_2$}FeBr]$_2$ (6). To a 100 mL round-bottom flask equipped with a stir bar were added $FeBr_2$ (1.58 g, 7.3 mmol) and THF (50 mL). The brown suspension was stirred for 1 h to dissolve most of the $FeBr_2$. To this brown solution was added dropwise a THF (20 mL) solution of [(^{i}Pr$_2$N)C(NDipp)$_2$]K (3.67 g, 7.3 mmol). An immediate color change to brown-gray with formation of insoluble gray particles was observed. The whole suspension was stirred at room temperature for 36 h. The suspension was filtered through Celite supported on a medium-porosity glass frit to remove most of the KBr. All volatiles were removed under reduced pressure to

DOI: 10.1021/acs.inorgchem.5b01815
Inorg. Chem. 2015, 54, 10030−10041

afford a brown semisolid. To this was added hexane (5 mL), and all the volatiles were removed under reduced pressure to afford a brown powder. To this was added hexane (50 mL), and the solution refiltered. The filtrate was concentrated (ca. 10 mL) and kept at −25 °C for 2 days to afford brown crystals. Yield: 3.5 g, 79%. ^{1}H NMR (25 °C, 300 MHz, C_6D_6): δ −28.7 (s, 12H, CHMe_2), −20.7 (s, 2H), 4.62 (s, 12H, CHMe_2), 16.81 (s, 12H, CHMe_2), 19.03 (s, 4H), 24.94 (s, 4H), 57.82 (s, 2H). IR (KBr pellet, cm^{-1}): 3365 (w), 3057 (m), 2959 (s), 2925 (s), 2867 (m), 1610 (m), 1582 (m), 1457 (s), 1432 (s), 1373 (s), 1279 (m), 1245 (m), 1173 (w), 1124 (s), 1109 (m), 1046 (w), 936 (w), 932 (w), 873 (w), 795 (m), 753 (s), 722 (w), 660 (w), 581 (w), 512 (w), 426 (w). μ_{eff} (Evans, C_6D_6, 298 K): 6.5 μ_B. Anal. Calcd $C_{62}H_{96}Br_2Fe_2N_6$: C, 62.21; H, 8.08; N, 7.02. Found: C, 62.12; H, 8.05; N, 7.06.

Synthesis of [(^{i}Pr$_2$N)*C*(NDipp)$_2$]Fe(η^6-C$_7$H$_8$) (9). To a 20 mL scintillation vial containing a small stir bar were added **6** (200 mg, 0.17 mmol), activated magnesium turnings (40 mg, 1.6 mmol), and toluene (9 mL). To this was added THF (1 mL), and the reaction mixture was stirred vigorously for 72 h. A color change from pale yellow-brown to deep red was observed over this period. Subsequently, the solution was filtered through Celite supported on a medium-porosity glass frit to remove excess magnesium turnings and most of the $MgBr_2$. All volatiles were removed under reduced pressure to afford a dark red semisolid. To this was added hexane (15 mL), and the solution again filtered. The filtrate was concentrated (ca. 2 mL) and kept at −25 °C for 2 days to afford deep red crystals. Yield: 150 mg, 72%. ^{1}H NMR (25 °C, 400 MHz, C_6D_6): δ 0.0 (s, 12H, CHMe_2), 1.4 (s, 12H, CHMe_2), 2.1 (s, 3H, Ph*Me*), 2.6 (br s, 12H, CHMe_2), 6.3 (s, 4H, *CH*Me$_2$), 11.3 (s, 2H, *CH*Me$_2$), six Ar*H* resonances not observed. IR (KBr pellet, cm^{-1}): 3048 (w), 2958 (s), 2925 (s), 2865 (m), 1612 (w), 1582 (w), 1446 (s), 1435 (s), 1407 (s), 1385 (s), 1316 (m), 1314 (m), 1276 (m), 1240 (m), 1203 (w), 1175 (m), 1125 (m), 1106 (m), 1054 (w), 1045 (w), 1025 (w), 988 (w), 986 (w), 933 (w), 872 (w), 799 (m), 789 (w), 774 (w), 755 (w), 728 (w), 725 (w), 694 (w), 659 (w), 640 (w), 523 (w), 431 (w). μ_{eff} (Evans, C_6D_6, 298 K): 2.4 μ_B. Anal. Calcd $C_{38}H_{56}FeN_3$: C, 74.73; H, 9.24; N, 6.88. Found: C, 74.48; H, 9.29; N, 6.76.

Synthesis of [{μ-(^{t}Bu$_2$CN)*C*(NDipp)$_2$}$_2$Fe$_2$] (11). To a 20 mL scintillation vial containing a small stir bar were added **5**-^{t}**Bu** (244 mg, 0.19 mmol), toluene (6 mL), and two drops of THF. In another 20 mL scintillation vial was added KC_8 (55 mg, 0.40 mmol) and toluene (4 mL). Both solutions were frozen. Upon thawing, the KC_8 suspension was added dropwise to the **5**-^{t}**Bu** solution with vigorous stirring. The reaction was allowed to warm to room temperature slowly over a 5−6 h period. A color change from yellow to dark red was observed during this time. Once all the KC_8 was consumed, the solution was filtered through Celite supported on a medium-porosity glass frit to remove most of the KBr. All volatiles were removed under reduced pressure to afford a dark red semisolid. To this was added Et_2O (10 mL), and the solution again filtered to remove remaining KBr. The filtrate was concentrated (ca. 2 mL) and kept at −25 °C for 2 days to afford deep dark red crystals. Yield: 140 mg, 66%. ^{1}H NMR (25 °C, 400 MHz, C_6D_6): δ −33.9 (br s, 4H), −17.4 (s, 2H), 11.3 (s, 18H, N=C^t*Bu*$_2$), 15.0 (s, 4H), 20.2 (s, 24H, CHMe_2). IR (KBr pellet, cm^{-1}): 3058 (w), 2963 (s), 2870 (m), 1680 (s), 1433 (s), 1382 (s), 1325 (m), 1273 (m), 1249 (m), 1107 (w), 1048 (w), 972 (m), 931 (w), 894 (w), 792 (m), 749 (m), 728 (w), 616 (w), 566 (m), 543 (m). Anal. Calcd $C_{68}H_{104}Fe_2N_6$: C, 73.10; H, 9.38; N, 7.52. Found: C, 71.08; H, 9.44; N, 7.07.

Cyclic Voltammetry. Cyclic voltammetric measurements were performed using a CH Instruments 600e potentiostat with a PC unit controlled with CHI software (version 13.12). Experiments were performed in a glovebox under an inert N_2 atmosphere using platinum disks (2 mm diameter) embedded in Kel-F thermoplastic as the counter and working electrodes, while the reference electrode consisted of a platinum wire. Solutions utilized in the electrochemical studies were approximately 1 mM in complex with [NBu_4][PF_6] (0.1 M, THF) as supporting electrolyte. All potentials are reported versus the [Cp_2Fe]$^{0/+}$ couple, referenced as internal standard.

X-ray Structure Solutions and Refinement. X-ray diffraction data were collected on a Bruker 3-axis platform diffractometer equipped with an APEX I CCD detector using a graphite monochromator with a Mo Kα X-ray source (α = 0.710 73 Å). The crystal was mounted on a Mitigen Kapton loop, coated in NVH oil, and maintained at 100(2) K under a flow of nitrogen gas during data collection. A hemisphere of data was collected using ω and φ scans with 0.3° frame widths. Data collection and cell parameter determination were conducted using the SMART[37] program. Integration of the data and final cell parameter refinements were performed using SAINT[38] software with data absorption correction implemented through SADABS.[39] Structures were solved using direct, charge flipping, or structure expansion methods and difference Fourier techniques. All hydrogen atom positions were idealized and rode on the atom. Structure solution, refinement, graphics, and creation of publication materials were performed using SHELXTL[40] or the Olex2[41] crystallographic package.

The cocrystallized toluene molecule in **11** lies on an inversion center, which leads to positional disorder upon symmetry generation. This disorder was addressed by fixing one C−C bond length using the DFIX command and assigning 50% occupancies to the disordered carbon atoms.

■ ASSOCIATED CONTENT

Supporting Information

The Supporting Information is available free of charge on the ACS Publications website at DOI: 10.1021/acs.inorgchem.5b01815.

NMR, IR, and mass spectral data (PDF)
X-ray crystallographic information (CIF)
X-ray crystallographic information (CIF)
X-ray crystallographic information (CIF)
X-ray crystallographic information (CIF)
X-ray crystallographic information (CIF)
X-ray crystallographic information (CIF)
X-ray crystallographic information (CIF)

■ AUTHOR INFORMATION

Corresponding Author

*E-mail: asfortier@utep.edu.

Notes

The authors declare no competing financial interest.

■ ACKNOWLEDGMENTS

This research was funded in large part by the University of Texas at El Paso with added support provided by the National Science Foundation (NSF) PREM program (DMR-1205302). Leonel Griego is thanked for preliminary experiments contributing to this work.

■ REFERENCES

(1) Jones, C. *Coord. Chem. Rev.* **2010**, *254*, 1273.
(2) Edelmann, F. T. Chapter 3, Advances in the Coordination Chemistry of Amidinate and Guanidinate Ligands In *Advances in Organometallic Chemistry*; Anthony, F. H., Mark, J. F., Eds.; Academic Press, 2008; Vol. *57*, p 183.
(3) Coles, M. P. *Dalton Trans.* **2006**, 985.
(4) Junk, P. C.; Cole, M. L. *Chem. Commun.* **2007**, 1579.
(5) Bailey, P. J.; Pace, S. *Coord. Chem. Rev.* **2001**, *214*, 91.
(6) Zuyls, A.; Roesky, P. W.; Deacon, G. B.; Konstas, K.; Junk, P. C. *Eur. J. Org. Chem.* **2008**, *2008*, 693.
(7) Feil, F.; Harder, S. *Eur. J. Inorg. Chem.* **2005**, *2005*, 4438.
(8) Chlupatý, T.; Růžička, A. *Coord. Chem. Rev.* **2015**, DOI: 10.1016/j.ccr.2015.07.012.

DOI: 10.1021/acs.inorgchem.5b01815
Inorg. Chem. 2015, 54, 10030−10041

(9) Cole, M. L.; Deacon, G. B.; Junk, P. C.; Wang, J. *Organometallics* **2013**, *32*, 1370.
(10) Deacon, G. B.; Junk, P. C.; Macreadie, L. K.; Werner, D. *Eur. J. Inorg. Chem.* **2014**, *2014*, 5240.
(11) Asay, M.; Jones, C.; Driess, M. *Chem. Rev.* **2011**, *111*, 354.
(12) Hicks, J.; Jones, C. *Inorg. Chem.* **2013**, *52*, 3900.
(13) Lane, A. C.; Vollmer, M. V.; Laber, C. H.; Melgarejo, D. Y.; Chiarella, G. M.; Fackler, J. P.; Yang, X.; Baker, G. A.; Walensky, J. R. *Inorg. Chem.* **2014**, *53*, 11357.
(14) Kelley, M. R.; Rohde, J.-U. *Inorg. Chem.* **2013**, *52*, 2564.
(15) Werner, D.; Deacon, G. B.; Junk, P. C.; Anwander, R. *Chem. - Eur. J.* **2014**, *20*, 4426.
(16) Maity, A. K.; Fortier, S.; Griego, L.; Metta-Magaña, A. J. *Inorg. Chem.* **2014**, *53*, 8155.
(17) Coles, M. P. *Chem. Commun.* **2009**, 3659.
(18) Lewis, R. A.; George, S. P.; Chapovetsky, A.; Wu, G.; Figueroa, J. S.; Hayton, T. W. *Chem. Commun.* **2013**, *49*, 2888.
(19) Lewis, R. A.; Wu, G.; Hayton, T. W. *J. Am. Chem. Soc.* **2010**, *132*, 12814.
(20) Carmalt, C. J.; Newport, A. C.; O'Neill, S. A.; Parkin, I. P.; White, A. J. P.; Williams, D. J. *Inorg. Chem.* **2005**, *44*, 615.
(21) Schmidt, J. A. R.; Arnold, J. *Chem. Commun.* **1999**, 2149.
(22) Xia, A.; El-Kaderi, H. M.; Jane Heeg, M.; Winter, C. H. *J. Organomet. Chem.* **2003**, *682*, 224.
(23) Jin, G.; Jones, C.; Junk, P. C.; Lippert, K.-A.; Rose, R. P.; Stasch, A. *New J. Chem.* **2009**, *33*, 64.
(24) Rose, R. P.; Jones, C.; Schulten, C.; Aldridge, S.; Stasch, A. *Chem. - Eur. J.* **2008**, *14*, 8477.
(25) Allen, F. H.; Kennard, O.; Watson, D. G.; Brammer, L.; Orpen, A. G.; Taylor, R. *J. Chem. Soc., Perkin Trans. 2* **1987**, S1.
(26) Buhmann, M.; Würthwein, E.-U.; Möller, M. H.; Rodewald, U. *Chem. Ber.* **1993**, *126*, 2467.
(27) Heße, N.; Fröhlich, R.; Wibbeling, B.; Würthwein, E.-U. *Eur. J. Org. Chem.* **2006**, *2006*, 3923.
(28) Noor, A.; Bauer, T.; Todorova, T. K.; Weber, B.; Gagliardi, L.; Kempe, R. *Chem. - Eur. J.* **2013**, *19*, 9825.
(29) Fohlmeister, L.; Liu, S.; Schulten, C.; Moubaraki, B.; Stasch, A.; Cashion, J. D.; Murray, K. S.; Gagliardi, L.; Jones, C. *Angew. Chem., Int. Ed.* **2012**, *51*, 8294.
(30) As a crude, powdered product, **12** is highly soluble in aromatic solvents. However, after purification by crystallization, its solubility in aromatics decreases signficantly.
(31) Fohlmeister, L.; Jones, C. *Aust. J. Chem.* **2014**, *67*, 1011.
(32) Clegg, W.; Snaith, R.; Shearer, H. M. M.; Wade, K.; Whitehead, G. *J. Chem. Soc., Dalton Trans.* **1983**, 1309.
(33) Lewis, R. A. Ph.D. Thesis, University of California, Santa Barbara, CA, 2013.
(34) Odom, A. L.; Cummins, C. C. *Organometallics* **1996**, *15*, 898.
(35) Findlater, M.; Hill, N. J.; Cowley, A. H. *Dalton Trans.* **2008**, 4419.
(36) Cole, M. L.; Jones, C.; Junk, P. C.; Kloth, M.; Stasch, A. *Chem. - Eur. J.* **2005**, *11*, 4482.
(37) *SMART Apex II*, Version 2.1; Bruker AXS Inc.: Madison, WI, 2005.
(38) *SAINT Software User's Guide*, Version 7.34a; Bruker AXS Inc.: Madison, WI, 2005.
(39) Blessing, R. *Acta Crystallogr., Sect. A: Found. Crystallogr.* **1995**, *A51*.3310.1107/S0108767394005726
(40) Sheldrick, G. M. *SHELXTL, 6.12*; Bruker Analytical X-Ray Systems, Inc.: Madison, WI, 2001.
(41) Dolomanov, O. V.; Bourhis, L. J.; Gildea, R. J.; Howard, J. A. K.; Puschmann, H. *J. Appl. Crystallogr.* **2009**, *42*, 339.

DOI: 10.1021/acs.inorgchem.5b01815
Inorg. Chem. 2015, 54, 10030−10041